A multilevel electrolyte-gated artificial synapse based on ruthenium-doped cobalt ferrite

P. Monalisha [1,2], Shengyao Li [2], Tianli Jin [2], P. S. Anil Kumar [1], S. N. Piramanayagam [2,]*

[1]Department of Physics, Indian Institute of Science, Bangalore, India, 560012

[2]Division of Physics and Applied Physics, School of Physical and Mathematical Sciences, Nanyang Technological University, 637371, Singapore

Email: prem@ntu.edu.sg

Abstract:

Synaptic devices that emulate synchronized memory and processing are considered the core components of neuromorphic computing systems for the low-power implementation of artificial intelligence. In this regard, electrolyte-gated transistors (EGTs) have gained much scientific attention, having a similar working mechanism as the biological synapses. Moreover, compared to a traditional solid-state gate dielectric, the liquid dielectric has the key advantage of inducing extremely large modulation of carrier density while overcoming the problem of electric pinholes, that typically occurs when using large-area films gated through ultra-thin solid dielectrics. Herein we demonstrate a three-terminal synaptic transistor based on ruthenium-doped cobalt ferrite (CRFO) thin films by electrolyte gating. In the CRFO-based EGT, we have obtained multilevel non-volatile conductance states for analog computing and high-density storage. Furthermore, the proposed synaptic transistor exhibited essential synaptic behavior, including spike amplitude-dependent plasticity (SADP), spike duration-dependent plasticity (SDDP), long-term potentiation (LTP), and long-term depression (LTD) successfully by applying electrical pulses. This study can motivate the development of advanced neuromorphic devices that leverage simultaneous modulation of electrical and magnetic properties in the same device and show a new direction to synaptic electronics.

Keywords:

Cobalt ferrite, artificial synapse, multilevel states, electrolyte gating, neuromorphic device

Introduction

The brain-inspired neuromorphic computing (NC), facilitates parallel processing for artificial neural networks (ANNs) with lower energy consumption [1,2]. There has been aroused research interest for NC due to limitations imposed by the von Neumann bottleneck (separately placed memory and logic units) that waste excessive energy in data transmission, facing energy and speed inefficiency. However, the synapse in the human brain offers synchronized memory and processing. Inspired by this, the research on synaptic devices that emulate the function and working mechanism of the synapse has been extensively investigated in recent years [3,4]. In this regard, many two-terminal (2T) synaptic devices such as memristors [5], phase-change memory [6], atom switches [7], etc., have been explored. Although 2T synaptic devices are suitable for easy and large-scale integration, they face challenges due to coupled reading and writing through the same terminals.

The aforementioned problems were taken care of by the three-terminal (3T) synaptic device, where the writing is carried out using voltage pulses applied on the gate terminal with the advantage of independent reading and writing. Recently, various field-effect transistors (FETs)-based, 3T synaptic devices have been proposed to emulate synaptic behavior, such as ferroelectric FETs (FeFETs) [8], electrolyte-gated transistors (EGTs) [9,10][11], and floating gate transistors (FGTs) [12], etc. Among various 3T devices, EGTs have gained much attention, having a similar working mechanism as the biological synapse. In terms realization of neuromorphic architecture, EGT offers significant advantages due to ultralow-voltage operation and the ability to form parallel-interconnected networks with minimal hardwired connectivity [13]. Compared to 2T liquid-based resistive synapses, the 3T EGT offers high stability, linear conductance modulation, and desirable weight-controllability [14–16]. Recently many functional oxide thin films such as $SrFeO_3$ [17], VO_2 [18], and $SrCoO_3$[19] have been used as the channel material in EGTs.

Cobalt ferrite ($CoFe_2O_4$) is a well-known functional oxide, with an inverse spinel structure that has been explored extensively for its magnetic behavior. It exhibits perpendicular magnetic anisotropy (PMA) when grown on MgO substrate due to stress anisotropy; however, its insulating nature restricts its usage [20]. As a solution, ruthenium (Ru) doping in cobalt ferrite (CRFO) decreases its resistivity by orders of magnitude while retaining its magnetic properties intact [21]. In CRFO, Ru^{4+} substitute for Co^{2+} and converts Fe^{3+} to Fe^{2+} to maintain charge neutrality, which increases the electrical conductance by hopping of t_{2g} electrons [22]. Furthermore, with electrolyte gating of CRFO, the ion insertion/extraction leads to further conversion of Fe^{3+} to Fe^{2+} and vice versa, leading to the tuning of electrical conductance. Electrolyte gating of cobalt ferrite has been studied recently, to tune the magnetic properties through voltage-driven ion migration, for low-power memory applications [23]. Apart from the fundamental studies, CRFO has extensive technological applications in spin filters [24], resistive switching [25], magneto-electronic devices [26], supercapacitors [27], magneto-optic media [28], biomedical devices [29], and high-density storage device [30], etc.

In most of the studies on NC, only the channel conductance has been tuned to mimic synaptic functionalities. In some recent studies, only the magnetic properties such as magnetization [31,32], and anomalous hall resistance [33], have been tuned. However, a magnetic oxide semiconductor such as CRFO motivates the tuning of both magnetic and electrical properties in the same device, for advanced NC applications, where along with the channel conductance, the sample magnetization (considered as synaptic weight) can be tuned by electrolyte gating, which is promising for future spin-based multifunctional synaptic devices [34]. In addition, the additional degree of freedom provided by the vector nature of magnetization can be exploited to toggle the polarity of synaptic weight without the need for additional electronics [31,33].

In this work, we have demonstrated ruthenium-doped cobalt ferrite-based three-terminal synaptic device by ionic liquid gating. We have obtained multilevel, non-volatile conductance states for analog computing and ultra-high-density memory applications. Our synaptic device exhibited essential synaptic behaviors, including spike amplitude-dependent plasticity (SADP), spike duration-dependent plasticity (SDDP), long-term potentiation (LTP), and long-term depression (LTD). This study can motivate the development of advanced neuromorphic devices that leverage modulation of both electrical and magnetic properties in the same device to enhance the device performance for future neuromorphic computing applications.

Experimental details:

Epitaxial thin films of Ru doped cobalt ferrite- CRFO (001) were grown on 5 mm × 5mm × 0.5 mm MgO (001) substrates using the pulsed laser deposition (PLD) technique. The PLD system used a KrF excimer laser (λ = 248 nm). The laser was focused on the rotating target with an energy fluence of ~1.2 J/cm^2 and was fired with a repetition rate of 3 Hz. The films were grown at a substrate temperature of 600 ^{o}C in a vacuum of 10^{-5} mbar. The films were in-situ annealed at 450 ^{o}C for one hour and cooled down to room temperature at 5 ^{o}C/minute. The CRFO film has a thickness of ~ 40 nm.

The channel with a length of 1500 µm and a width of 150 µm was patterned using photolithography and was etched using argon ion milling. The three-terminal coplanar gated electrode of Cr (5 nm)/ Au (55 nm) was deposited via thermal evaporation. We have used ionic liquid (IL) as the gate dielectric, due to higher ionic mobility, larger electrochemical window (several volts), and lower vapor pressure. N, N-diethyl-N-methyl-N-(2-methoxyethyl) ammonium bis(trifluoromethanesulfonyl)imide (DEME-TFSI) is a commonly used IL due to its smaller ionic radii, which results in high specific capacitance. For the present study, as received DEME-TFSI IL from Canto chemical was used as the gate electrolyte. All the electrical measurements of the CRFO-based synaptic transistor were carried out using Lakeshore Janis ST300 compact cryostats at room temperature. All the electrical measurements were carried out in a vacuum of 10^{-3} mbar to protect the IL from ambient. A constant DC was applied across the channel using the Yokagawa GS20 DC source, and the potential drop was measured using Keithley 2000 multimeter. Meanwhile, the gate voltage pulses were applied using Keithley 6517B electrometer.

Results and Discussion:

Device Operation:

Herein, we proposed a three-terminal synaptic device based on ruthenium-doped cobalt ferrite thin film by IL gating. Figure 1a shows the schematics to demonstrate the analogy between the proposed artificial synapse and the biological synapse. Depending on the activity level the synaptic weight is tuned, giving rise to a phenomenon termed synaptic plasticity, which plays a critical role in the learning and memory of the human brain [35],[36]. The structure and working mechanism of the IL-gated synaptic transistor have a close resemblance to its biological counterpart. In the synaptic device (Figure 1a, right), the channel conductance represents the synaptic weight, which can be tuned by electrolyte gating to emulate several

synaptic behaviors. Hence, an electrolyte-gated CRFO-based three-terminal synaptic transistor offers a flexible way to emulate synaptic behavior in an electronic device.

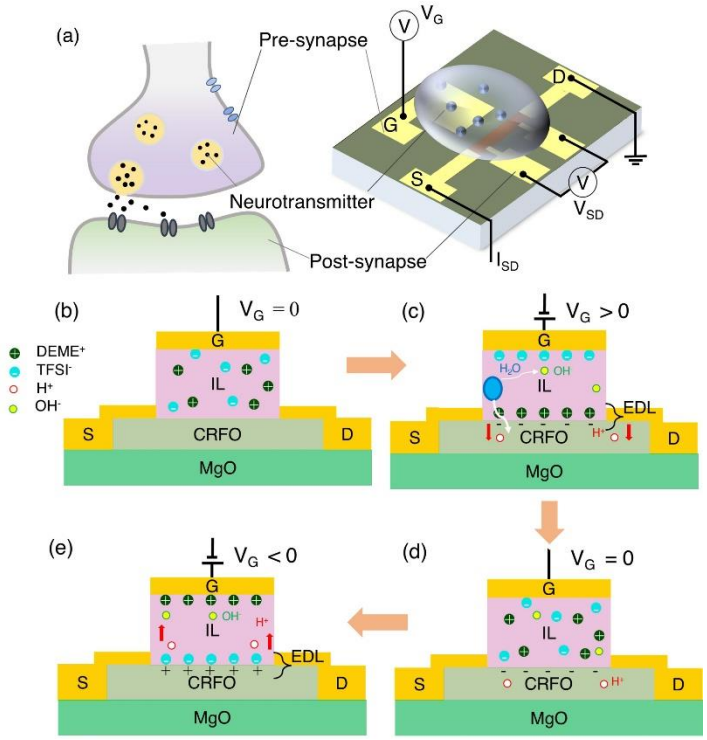

Figure 1 (a) Schematic demonstration of analogy between biological synapse and CRFO-based artificial synapse by electrolyte gating. Schematics of proposed working mechanism (b) Equilibrium state of the synaptic device at no gating condition. (c) With positive gating, an electric double layer (EDL) formed at the interface and inject the H^+ ion (proton) into the CRFO channel. (d) The process is nonvolatile; the H^+ ion is retained inside the channel even at zero gating condition. (e) The H^+ ions are extracted from the CRFO channel surface with negative gating.

Figure 1a (right) shows the electrical measurement setup of the device. A small direct current I_{SD} = 2 µA was applied across the source and drain electrode for the four-probe electrical measurements. The potential drop across the channel was measured and converted to channel conductance ($G = V_{SD}/I_{SD}$). Meanwhile, the pulsed gate voltages were directly applied to the in-plane gate electrode. Furthermore, the corresponding leakage current I_G was measured across the gate and drain terminal. The drain terminal was grounded throughout the measurement. The electrode contact quality was checked by the current-voltage measurement, and it exhibited a linear relationship indicating good ohmic contacts (Figure S1a in Supporting Information). The gate dielectric (IL) was characterized by the frequency-dependent specific capacitance measurement, as shown in Figure S1b. We have obtained the highest capacitance of 6.9 µF/ cm^2 at 30 Hz, claiming its ability for massive carrier accumulation at the interface.

A tiny drop of DEME-TFSI IL was dropped over the device, covering the channel and a larger part of the gate electrode.

The study of IL gating is widespread in the functional oxide thin film community for its exotic behavior in various materials [37,38],[39,40],[41]. The phenomenal behavior is attributed to massive carrier injection at very low voltage. Figure 1(b-e) shows the schematic illustration of the proposed working mechanism of CRFO-based synaptic transistor. The ions are distributed randomly at no gating condition (Figure 1b). On gating, the electric field forces the mobile ions to segregate and accumulate at the channel /IL interface, forming an electric double layer (EDL) that induces charge carriers in the channel by electrostatic induction. Furthermore, it has been known that the IL contains small traces of water that undergo hydrolysis reaction above a threshold ($V_T \sim 1.5$ V) [42], releasing H^+ (proton) and OH^- (hydroxyl) ions. We propose that being smaller in size and having high chemical activity, the protons play a crucial role in electrochemical doping in the CRFO channel [43–47]. Adding to the EDL formation, electrochemical doping of the channel occurs with gating. During positive gating, the H^+ ion intercalates into the channel assisted by the positive electric field (Figure 1c). The inserted H^+ ion remains intact in the channel, even at zero gating, as shown in Figure 1d showing the non-volatile change. An external electric field of opposite polarity is needed to extract the H^+ ions from the channel. During negative gating, the opposite electric field assists H^+ ion extraction from the channel (Figure 1e). This process of conductance modulation is reversible and resembles the signal transmission process of a synapse.

The water content in the IL is very low [48][49], and also the water content strongly depends on the vacuum degree.[50] As the experiments were carried out in a vacuum (10^{-3} mbar) and with minimal water content in the IL, any oxygen bubble evolution or substantial change in pH of the IL is essentially not expected in the present case.

Performance Characteristics:

Figure 2a shows the channel conductance variation as a function of the gate voltage curve for the CRFO-based synaptic transistor. It was measured by sweeping the gate voltage in an anticlockwise fashion from 0 to 3 V, 3 to -3.1 V, and back to 0 V at a sweeping speed of 0.008 V/s. The channel conductance vs. gate voltage curve demonstrated a large anticlockwise hysteresis loop, implying a reversible and non-volatile modulation of the channel conductance between the high and low conductance states. This indicates the potential application of the device for synaptic function emulation.

The hysteric behavior in the G vs. V_G curve can be explained as follows. With gating, along with the EDL formation, electrochemical doping of the channel occurs. During positive gating, (Figure 2a path ①and ②), proton is inserted into the channel assisted by the positive electric field. With proton insertion, Fe^{3+} is converted to Fe^{2+} in the channel, which increases the channel conductance by increasing the hopping of t_{2g} electrons from Fe^{2+} to Fe^{3+}. The inserted protons remain intact in the channel, even at zero gating giving

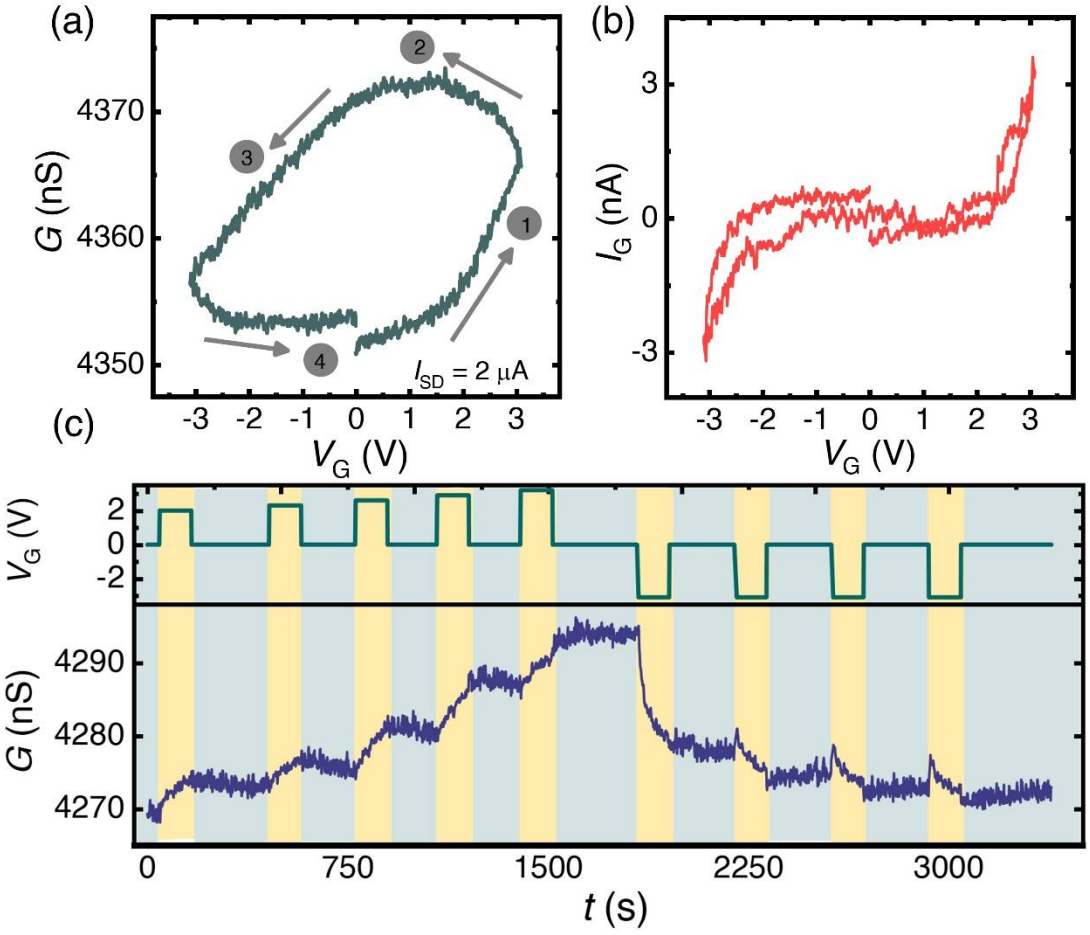

Figure 2 (a) Channel conductance variation as a function gate voltage, by anticlockwise sweeping of V_G from 0 to 3 V, 3 to -3.1 V, and back to 0 V with a sweeping rate of 0.008 V/s, I_{SD} = 2μA. (b) The leakage current (I_G) was measured as a function of V_G. (c) Distinct multilevel and non-volatile conductance states were obtained by applying a series of gate pulses of different amplitudes, I_{SD} = 2 μA.

nonvolatility. Conversely, during negative gating proton is extracted from the channel aided by the negative electric field. With negative gating (Figure 2a path ③ and ④), proton extraction causes the back conversion of Fe^{2+} to Fe^{3+}, which decreases the channel conductance, bringing it back to the initial state. The electrochemical doping results in a non-volatile change in channel conductance, shown by different G values at V_G= 0 in Figure 2a. The reversibility of the electrochemical doping makes the reversible channel conductance modulation possible,

resulting in a closed-loop behavior. Furthermore, the hysteric behavior in the transfer curve indicates the slow kinetics of the ions. The simultaneously measured leakage current (I_G) is shown in Figure 2b. It shows a minimum I_G ~ 2 nA (three orders of magnitude lower than I_{SD}) even at the highest gate voltage, assuring an active gate–channel coupling.

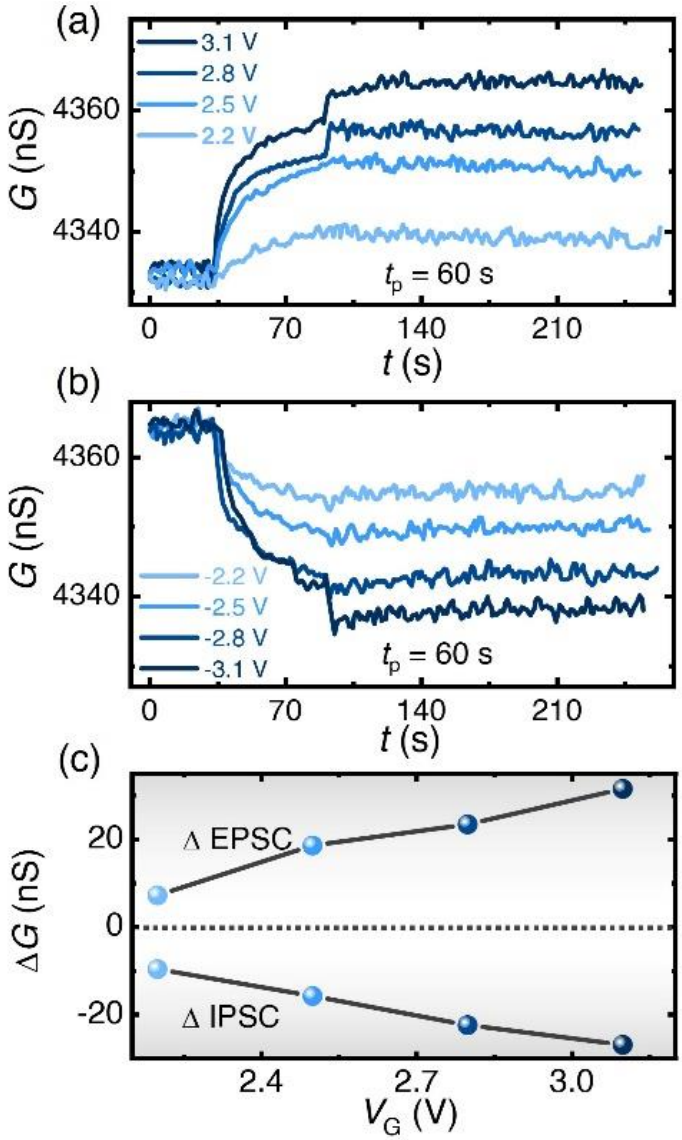

Figure 3: Spike amplitude-dependent plasticity (SADP) (a) EPSC response of a series of positive spikes of the same duration (t_p = 60 s) and different amplitudes (V_G = 2.2, 2.5, 2.8, and 3.1 V), I_{SD} = 2 µA. (b) IPSC response of a series of negative spikes of the same duration (t_p = 60 s) and different amplitudes (V_G = -2.2, -2.5, -2.8, and -3.1 V), I_{SD} = 2 µA. (c) Summarized value ΔG as a function of spike amplitude in both excitatory and inhibitory modes.

Multilevel non-volatile conductance states are necessary for analog computing and emulation of synaptic behavior. It also aids in ultra-high-density memory applications. In our CRFO-

based synaptic transistor, we have realized multilevel non-volatile conductance states by applying a series of positive gate pulses of different amplitudes (in the sequence of V_G = 2.0, 2.3, 2.6, 2.9, and 3.2 V, t_p = 120 s), with a time interval of Δt = 180 s, where information can be stored in the multilevel states (Figure 2c). The channel conductance increased during positive gating and retained the same state during zero gating, showing the intrinsic non-volatile nature of the distinct states. We have realized a stepped increment in channel conductance in six distinct non-volatile states during the writing process. The channel conductance was brought back to the initial state by applying a series of negative gate pulses (V_G = -3.2 V, t_p = 30 s), spaced apart by Δt = 240 s. The channel conductance decreased in a stepped manner in four distinct non-volatile states to its original value during erasing. The multilevel behavior can be explained based on different levels of electrochemical doping with controlled insertion/extraction of protons into/out of the CRFO channel using a programmed gate pulse. The CRFO-based artificial synapse exhibited distinct multilevel states during both the writing and erasing processes.

In the biological synapse, the external stimuli trigger a potential drop across the post-synaptic membrane, called post-synaptic potential (PSP). In our CRFO-based artificial synapse, the PSP exhibits the form of a change in channel conductance called post-synaptic conductance (PSC) [51]. In the implementation of artificial synapses, the increment in channel conductance can be used to emulate excitatory post-synaptic conductance (EPSC). Analogously the decrement in channel conductance can be used to emulate the inhibitory post-synaptic conductance (IPSC). Both EPSC and IPSC are crucial for the signal transmission process in the neuronal network.

Figure 3 demonstrates an important synaptic behavior called spike amplitude-dependent plasticity (SADP), demonstrating the tuning of synaptic plasticity via spike amplitude. We have recorded EPSC induced by a series of positive spikes of identical duration time (t_p = 60s) and different amplitudes (2.2, 2.5, 2.8, and 3.1 V), as shown in Figure 3a. The EPSC peak increased with increasing spike amplitude and retained the higher conductance state showing the highly non-volatile nature of the conductance modulation. The conductance modulation ΔG was calculated for each pulse as the difference between the base (V_G = 0) and peak value. For the EPSC mode, the ΔG increased linearly with increasing spike amplitude, as shown in Figure 3c (upper panel). In contrast, IPSC induced by a series of negative spikes of identical duration time (t_p = 60 s) and different amplitudes (-2.2, -2.5, -2.8, and -3.1 V) is shown in Figure 3b. The IPSC peak value and retention increased (downward) for a more negative spike amplitude. For the IPSC mode, the ΔG increased (downward) with increasing spike amplitudes, as shown

in Figure 3c (lower panel). The variation of Δ*G* for both EPSC and IPSC modes with spike amplitude is summarized in Figure 3c. The conductance modulation (Δ*G*) increased linearly with increasing spike amplitude in both exhibitory and inhibitory modes. Such behavior in CRFO-based synaptic transistors was due to stronger electrochemical doping of the channel due

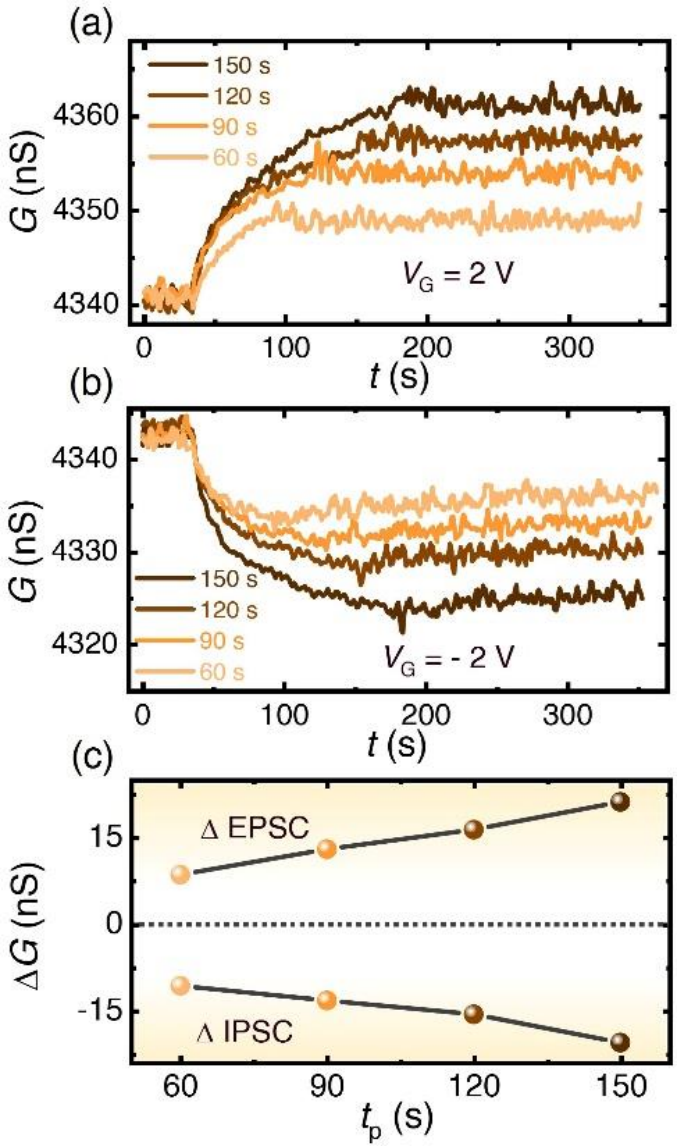

Figure 4: Spike duration-dependent plasticity (SDDP) (a) EPSC response of a series of positive spikes of the same amplitude (V_G = 2.5 V) and different durations (t_p = 60, 90, 120 and 150 s), I_{SD} = 2 µA. (b) IPSC response of a series of negative spikes of the same amplitude (V_G = -2.5 V) and different durations (t_p = 60, 90, 120, and 150 s), I_{SD} = 2 µA. (c) Summarized value Δ*G* as a function of spike durations for both excitatory and inhibitory modes

to intercalation/extraction of more protons into/out the channel at higher positive/negative spike amplitude.

Moreover, spike duration plays a significant role in tuning the synaptic plasticity, giving rise to spike duration-dependent plasticity phenomena (SDDP). The EPSC triggered by a series of positive spikes of the same amplitude (V_G = 2.5 V) and different durations (60, 90, 120, and 150 s) is shown in Figure 4a, using a constant I_{SD} = 2 µA. The EPSC peak has increased with increasing the spike duration. Furthermore, the channel conductance retained the higher state

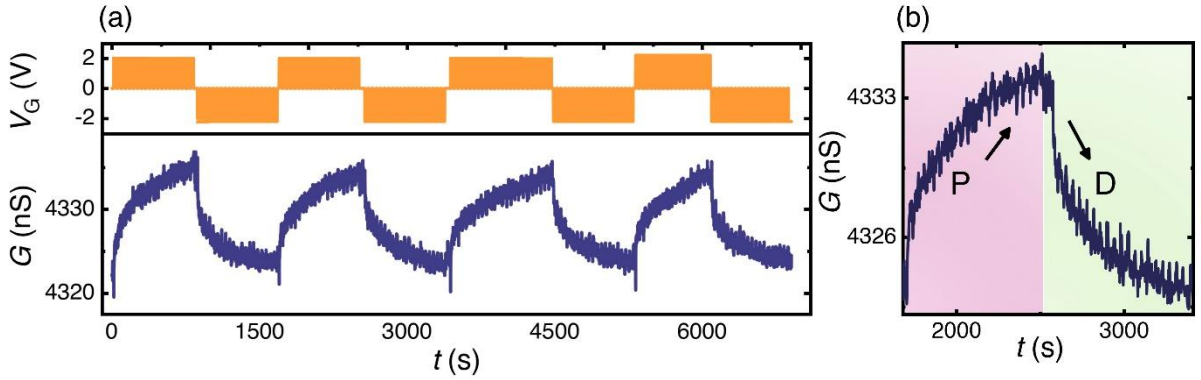

Figure 5: (a) Continuous cycles of long-term potentiation (LTP) and long-term depression (LTD) obtained by applying twenty consecutive positive spikes (V_G = 2 V, t_p = 30 s, Δt = 10 s) for potentiation, followed by twenty consecutive negative spikes (V_G = -2.2 V, t_p = 30 s, Δt = 10 s) for depression, I_{SD} = 2µA. (b) Enlarged view of a single cycle of potentiation and depression.

for each stimulus, showing complete non-volatile nature, making it suitable for long-term memory applications. The conductance modulation ΔG has increased with increasing the spike duration time for the EPSC mode, as shown in Figure 4c (upper panel). In contrast, the IPSC triggered by a series of negative spikes of the same amplitude (V_G = -2.5 V) and different durations (60, 90, 120, and 150 s) is shown in Figure 4b. The IPSC peak value has increased (downward) for the longer spike duration. The ΔG has increased (downward) for the IPSC mode (Figure 4c, lower panel).

The summarized value of conductance modulation (ΔG) is plotted in Figure 4c for excitatory and inhibitory modes, showing linear increments with increasing spike duration. The spike duration-dependent ΔG can be understood based on the electrochemical proton doping of the CRFO channel. A larger portion of the proton is injected/extracted into/out of the channel for a more extended positive/negative spike, causing more conductance modulation. This shows a successful demonstration of synaptic SDDP behavior in our device.

Long-term plasticity is defined as the persistent modification of synaptic weight that lasts from days to years. It is recognized as the biological basis for learning and long-term memory in the human brain at the cellular level [52–54]. Among the other synaptic functions, long-term

plasticity has been considered important as it exhibits a non-volatile memory effect, hence playing a significant role in image recognition and self-learning in NC. In the CRFO synaptic transistor, we mainly focus on emulating long-term phenomena due to the complete non-volatile nature of the conductance modulation. Long-term plasticity is demonstrated in the device via potentiation and depression of synaptic weight termed long-term potentiation (LTP) and long-term depression (LTD), respectively, exhibited by applying a series of electrical pulses on the gate terminal.

Figure 5a demonstrates continuous cycles of long-term potentiation and depression of synaptic weight by applying twenty consecutive positive spikes (V_G = 2 V, t_p = 30 s) with Δt = 10 s, followed by 20 consecutive negative spikes (V_G = -2.2 V, t_p = 30 s) with Δt = 10 s to modulate the channel conductance, under a constant I_{SD} = 2 µA. The channel conductance increased monotonously with consecutive positive spikes (potentiation) and was subsequently brought back to the initial state with negative spikes (depression). We have demonstrated several cycles of potentiation and depression, proving good cyclic tolerance and stable switching of the synaptic device [55]. Figure 5b showed zoomed view of a single cycle of potentiation and depression. During LTP, the channel conductance increased monotonously due to the intercalation of more protons into the CRFO channel with consecutive positive spikes**.** However, successive negative spikes decreased the channel conductance monotonously during LTD by extracting more protons from the CRFO channel.

Challenges and Future Prospective of the Current Design:

In the current design, the CRFO-based synaptic device faces some challenges that can be improved greatly for practical NC applications. For instance, the lower conductance modulation and the slower temporal response of the device can be improved drastically by 1) using a smaller channel thickness (~3-5 nm) [56], 2) reducing the channel length ($\Delta G \propto L_{Channel}$) [57], 3) using a nanoporous active material [58], and 4) using a vertical device structure [57], etc. The energy consumption ($E = I^2Rt_p$) of the present device is high (~ 2 µJ), which can be reduced considerably by lowering device resistance (R), passage current (I), and pulse width (t_p). Firstly, doping with more Ru makes the device more conductive, which lowers the device R and I [22], secondly with a faster temporal response, t_p is reduced. The longer retention and endurance could not be measured in the present device due to instrumental limitations.

Conclusions:

In conclusion, we have investigated a three-terminal artificial synapse based on semiconducting Ru-doped cobalt ferrite by electrolyte gating. The channel conductance of CRFO has been modulated gradually in a reversible and non-volatile manner. The proposed synaptic device can store information in multilevel non-volatile conductance states programmed by applying V_G pulses of different amplitudes. Essential synaptic behaviors such as spike amplitude-dependent plasticity (SADP), spike duration-dependent plasticity (SDDP), long-term potentiation (LTP), and long-term depression (LTD) have been successfully simulated in the synaptic device. The study of magnetic semiconductor-based artificial synapses can motivate the development of advanced neuromorphic devices that leverage simultaneous modulation of magnetic and electrical properties in the same device by electrolyte gating for future spin-based multifunctional synaptic devices.

Acknowledgments:

The authors acknowledge the support from the CRP grant NRF-CRP21-2018-0003 of the National Research Foundation (NRF), Singapore. SNP acknowledges the partial support from the Tier 2 grant MOE2019-T2-1-117 of the Ministry of Education (MOE) Singapore. PSAK acknowledges support from the Ministry of Education (MoE), India. PM thanks Pratiksha Trust, India, for the financial support. The authors thank Prof. X. Renshaw Wang for the fruitful discussion and for allowing us to use his facilities.

Conflict of Interest

The authors declare no conflict of interest.

References:

[1] Yu R, Li E, Wu X, Yan Y, He W, He L, Chen J, Chen H and Guo T 2020 Electret-Based Organic Synaptic Transistor for Neuromorphic Computing *ACS Appl. Mater. Interfaces* **12** 15446–55

[2] Sun J, Oh S, Choi Y, Seo S, Oh M J, Lee M, Lee W B, Yoo P J, Cho J H and Park J-H 2018 Optoelectronic Synapse Based on IGZO-Alkylated Graphene Oxide Hybrid Structure *Adv. Funct. Mater.* **28** 1804397

[3] Lenz J, del Giudice F, Geisenhof F R, Winterer F and Weitz R T 2019 Vertical, electrolyte-gated organic transistors show continuous operation in the MA cm−2 regime and artificial synaptic behaviour *Nat. Nanotechnol.* **14** 579–85

[4] Chen J, Zhu C, Cao G, Liu H, Bian R, Wang J, Li C, Chen J, Fu Q, Liu Q, Meng P, Li W, Liu F and Liu Z Mimicking Neuroplasticity via Ion Migration in van der Waals Layered Copper Indium Thiophosphate *Adv. Mater.* **n/a** 2104676

[5] Yan X, Zhao J, Liu S, Zhou Z, Liu Q, Chen J and Liu X Y 2018 Memristor with Ag-Cluster-Doped TiO2 Films as Artificial Synapse for Neuroinspired Computing *Adv. Funct. Mater.* **28** 1705320

[6] Kuzum D, Jeyasingh R G D, Lee B and Wong H S P 2012 Nanoelectronic programmable synapses based on phase change materials for brain-inspired computing *Nano Lett.* **12** 2179–86

[7] Nayak A, Ohno T, Tsuruoka T, Terabe K, Hasegawa T, Gimzewski J K and Aono M 2012 Controlling the Synaptic Plasticity of a Cu2S Gap-Type Atomic Switch *Adv. Funct. Mater.* **22** 3606–13

[8] Bragaglia V, Sousa M, Jan B, Abel S, Halter M, Be L, Luisier M and Fompeyrine J 2020 Back-End , CMOS-Compatible Ferroelectric Field-E ff ect Transistor for Synaptic Weights

[9] Xu W, Min S Y, Hwang H and Lee T W 2016 Organic core-sheath nanowire artificial synapses with femtojoule energy consumption *Sci. Adv.* **2** 1–8

[10] Monalisha P, Kumar P S A, Wang X R and Piramanayagam S N 2021 Emulation of Synaptic Plasticity on Cobalt based Synaptic Transistor for Neuromorphic Computing

[11] Monalisha P, Li S, Jin T, Kumar P S A and Piramanayagam S N 2022 Synaptic Plasticity Investigation in Permalloy based Channel Material for Neuromorphic Computing *J. Phys. D. Appl. Phys.*

[12] Kwon O, Oh S, Park H, Jeong S-H, Park W and Cho B 2022 In-depth analysis on electrical parameters of floating gate {IGZO} synaptic transistor affecting pattern recognition accuracy *Nanotechnology* **33** 215201

[13] Ling H, Koutsouras D A, Kazemzadeh S, Van De Burgt Y, Yan F and Gkoupidenis P 2020 Electrolyte-gated transistors for synaptic electronics, neuromorphic computing, and adaptable biointerfacing *Appl. Phys. Rev.* **7**

[14] Sun G, Slouka Z and Chang H-C 2015 Fluidic-Based Ion Memristors and Ionic Latches *Small* **11** 5206–13

[15] Ananthakrishnan A, Du X and Allen M G 2021 Water-based resistive switches for

neuromorphic long-range connections *J. Phys. D. Appl. Phys.* **54** 225104

[16] Kim D and Lee J-S 2019 Liquid-based memory and artificial synapse *Nanoscale* **11** 9726–32

[17] Shi P, Wang D, Yu T, Xing R, Wu Z, Yan S, Wei L, Chen Y, Ren H, Yu C and Li F 2021 Solid-state electrolyte gated synaptic transistor based on SrFeO2.5 film channel *Mater. Des.* **210** 110022

[18] Wu Z, Shi P, Xing R, Yu T, Zhao L, Wei L, Wang D, Yan S, Tian Y, Bai L and Chen Y Flexible Mott Synaptic Transistor on Polyimide Substrate for Physical Neural Networks *Adv. Electron. Mater.* **n/a** 2200078

[19] Huang H Y, Ge C, Zhang Q H, Liu C X, Du J Y, Li J K, Wang C, Gu L, Yang G Z and Jin K J 2019 Electrolyte-Gated Synaptic Transistor with Oxygen Ions *Adv. Funct. Mater.* **29** 1–8

[20] Niizeki T, Utsumi Y, Aoyama R, Yanagihara H, Inoue J I, Yamasaki Y, Nakao H, Koike K and Kita E 2013 Extraordinarily large perpendicular magnetic anisotropy in epitaxially strained cobalt-ferrite CoxFe3-xO4(001) (x = 0.75, 1.0) thin films *Appl. Phys. Lett.* **103** 0–5

[21] Peda M and Kumar P S A 2021 Magnetic and electrical transport properties of Ru doped cobalt ferrite thin films with perpendicular magnetic anisotropy *AIP Adv.* **11** 15346

[22] Iwamoto F, Seki M and Tabata H 2012 Magnetic and electric properties of Ru-substituted CoFe2O 4 thin films fabricated by pulsed laser deposition *J. Appl. Phys.* **112** 1–6

[23] Robbennolt S, Menéndez E, Quintana A, Gómez A, Auffret S, Baltz V, Pellicer E and Sort J 2019 Reversible, Electric-Field Induced Magneto-Ionic Control of Magnetism in Mesoporous Cobalt Ferrite Thin Films *Sci. Rep.* **9** 1–14

[24] Ramos A V, Guittet M-J, Moussy J-B, Mattana R, Deranlot C, Petroff F and Gatel C 2007 Room temperature spin filtering in epitaxial cobalt-ferrite tunnel barriers *Appl. Phys. Lett.* **91** 122107

[25] Hu W, Zou L, Chen R, Xie W, Chen X, Qin N, Li S, Yang G and Bao D 2014 Resistive switching properties and physical mechanism of cobalt ferrite thin films *Appl. Phys. Lett.* **104** 143502

[26] Chaudhuri A and Mandal K 2015 Large magnetoelectric properties in CoFe2O4:BaTiO3 core–shell nanocomposites *J. Magn. Magn. Mater.* **377** 441–5

[27] Kumbhar V S, Jagadale A D, Shinde N M and Lokhande C D 2012 Chemical synthesis of spinel cobalt ferrite (CoFe2O4) nano-flakes for supercapacitor application *Appl. Surf. Sci.* **259** 39–43

[28] Stichauer L, Gavoille G and Simsa Z 1996 Optical and magneto-optical properties of nanocrystalline cobalt ferrite films *J. Appl. Phys.* **79** 3645–50

[29] Srinivasan S Y, Paknikar K M, Bodas D and Gajbhiye V 2018 Applications of cobalt ferrite nanoparticles in biomedical nanotechnology *Nanomedicine* **13** 1221–38

[30] Nitika, Rana A and Kumar V 2021 Tailoring the Structural, Magnetic, Mechanical, and Thermal Properties of {CoFe}2O4 by Varying Annealing Temperature for High-

Density Storage Devices *{ECS} J. Solid State Sci. Technol.* **10** 31005

[31] Tan Z, de Rojas J, Martins S, Lopeandia A, Quintana A, Cialone M, Herrero-Martín J, Meersschaut J, Vantomme A, Costa-Krämer J L, Sort J and Menéndez E 2022 Frequency-dependent stimulated and post-stimulated voltage control of magnetism in transition metal nitrides: towards brain-inspired magneto-ionics *Mater. Horizons*

[32] Martins S, De Rojas J, Tan Z, Cialone M, Lopeandia A, Herrero-Martin J, Costa-Kramer J L, Menendez E and Sort J 2022 Dynamic electric-field-induced magnetic effects in cobalt oxide thin films: Towards magneto-ionic synapses *Nanoscale* **14** 842–52

[33] Mishra R, Kumar D and Yang H 2019 Oxygen-Migration-Based Spintronic Device Emulating a Biological Synapse *Phys. Rev. Appl.* **11** 1

[34] Li S, Miao B, Wang X, Teo S L, Lin M, Zhu Q, Piramanayagam S N and Wang X R 2022 Synaptic Modulation of Conductivity and Magnetism in a CoPt-Based Electrochemical Transistor **2200378** 1–7

[35] LYNCH M A 2004 Long-Term Potentiation and Memory *Physiol. Rev.* **84** 87–136

[36] Abbott L F and Nelson S B 2000 Synaptic plasticity: taming the beast *Nat. Neurosci.* **3** 1178–83

[37] Bollinger A T, Dubuis G, Yoon J, Pavuna D, Misewich J and BoŽović I 2011 Superconductor-insulator transition in La2-xSr xCuO4 at the pair quantum resistance *Nature* **472** 458–60

[38] Ueno K, Nakamura S, Shimotani H, Yuan H T, Kimura N, Nojima T, Aoki H, Iwasa Y and Kawasaki M 2011 Discovery of superconductivity in KTaO 3 by electrostatic carrier doping *Nat. Nanotechnol.* **6** 408–12

[39] Leng X, Garcia-Barriocanal J, Bose S, Lee Y and Goldman A M 2011 Electrostatic control of the evolution from a superconducting phase to an insulating phase in ultrathin YBa2Cu3O7-x films *Phys. Rev. Lett.* **107** 6–9

[40] Scherwitzl R, Zubko P, Lezama I G, Ono S, Morpurgo A F, Catalan G and Triscone J M 2010 Electric-field control of the metal-insulator transition in ultrathin NdNiO3 films *Adv. Mater.* **22** 5517–20

[41] Yi H T, Gao B, Xie W, Cheong S W and Podzorov V 2014 Tuning the metal-insulator crossover and magnetism in SrRuO3 by ionic gating *Sci. Rep.* **4**

[42] Yang J T, Ge C, Du J Y, Huang H Y, He M, Wang C, Lu H Bin, Yang G Z and Jin K J 2018 Artificial synapses emulated by an electrolyte-gated tungsten-oxide transistor *Adv. Mater.* **30** 1–10

[43] Deng X, Wang S Q, Liu Y X, Zhong N, He Y H, Peng H, Xiang P H and Duan C G 2021 A Flexible Mott Synaptic Transistor for Nociceptor Simulation and Neuromorphic Computing *Adv. Funct. Mater.* **2101099** 1–10

[44] Bisri S Z, Shimizu S, Nakano M and Iwasa Y 2017 Endeavor of Iontronics: From Fundamentals to Applications of Ion-Controlled Electronics *Adv. Mater.* **29** 1–48

[45] Ge C, Li G, Zhou Q li, Du J yu, Guo E jia, He M, Wang C, Yang G zhen and Jin K juan 2020 Gating-induced reversible HxVO2 phase transformations for neuromorphic

computing *Nano Energy* **67**

[46] Lu N, Zhang P, Zhang Q, Qiao R, He Q, Li H B, Wang Y, Guo J, Zhang D, Duan Z, Li Z, Wang M, Yang S, Yan M, Arenholz E, Zhou S, Yang W, Gu L, Nan C W, Wu J, Tokura Y and Yu P 2017 Electric-field control of tri-state phase transformation with a selective dual-ion switch *Nature* **546** 124–8

[47] Leng X, Pereiro J, Strle J, Dubuis G, Bollinger A T, Gozar A, Wu J, Litombe N, Panagopoulos C, Pavuna D and Božović I 2017 Insulator to metal transition in WO3 induced by electrolyte gating *npj Quantum Mater.* **2**

[48] Ge C, Jin K J, Gu L, Peng L C, Hu Y S, Guo H Z, Shi H F, Li J K, Wang J O, Guo X X, Wang C, He M, Lu H Bin and Yang G Z 2015 Metal-Insulator Transition Induced by Oxygen Vacancies from Electrochemical Reaction in Ionic Liquid-Gated Manganite Films *Adv. Mater. Interfaces* **2** 1–6

[49] Hope M A, Griffith K J, Cui B, Gao F, Dutton S E, Parkin S S P and Grey C P 2018 The Role of Ionic Liquid Breakdown in the Electrochemical Metallization of VO 2 : An NMR Study of Gating Mechanisms and VO 2 Reduction *J. Am. Chem. Soc.* **140** 16685–96

[50] Xu D D, Deng X, Zhao Y F, Ma R R, Zhong N, Huang R, Peng H, Xiang P H and Duan C G 2019 Hydrogenation Dynamics of Electrically Controlled Metal–Insulator Transition in Proton-Gated Transparent and Flexible WO3 Transistors *Adv. Funct. Mater.* **1902497** 1–9

[51] Pillai P B and De Souza M M 2017 Nanoionics-based three-terminal synaptic device using zinc oxide *ACS Appl. Mater. Interfaces* **9** 1609–18

[52] Pastalkova E, Serrano P, Pinkhasova D, Wallace E, Fenton A A and Sacktor T C 2006 Storage of Spatial Information by the Maintenance Mechanism of LTP *Science (80-.).* **313** 1141–4

[53] Whitlock J R, Heynen A J, Shuler M G and Bear M F 2006 Learning Induces Long-Term Potentiation in the Hippocampus *Science (80-.).* **313** 1093–7

[54] Xu W, Min S-Y, Hwang H and Lee T-W 2016 Organic core-sheath nanowire artificial synapses with femtojoule energy consumption *Sci. Adv.* **2**

[55] Fu Y, Kong L A, Chen Y, Wang J, Qian C, Yuan Y, Sun J, Gao Y and Wan Q 2018 Flexible Neuromorphic Architectures Based on Self-Supported Multiterminal Organic Transistors *ACS Appl. Mater. Interfaces* **10** 26443–50

[56] Tan Z, de Rojas J, Martins S, Lopeandia A, Quintana A, Cialone M, Herrero-Martín J, Meersschaut J, Vantomme A, Costa-Krämer J L, Sort J and Menéndez E 2022 Frequency-dependent stimulated and post-stimulated voltage control of magnetism in transition metal nitrides: towards brain-inspired magneto-ionics *Mater. Horizons*

[57] Lee C, Choi W, Kwak M, Kim S and Hwang H 2021 Excellent Synapse Characteristics of 50 nm Vertical Transistor with WOx channel for High Density Neuromorphic system *2021 Symposium on VLSI Technology* pp 1–2

[58] Robbennolt S, Menéndez E, Quintana A, Gómez A, Auffret S, Baltz V, Pellicer E and Sort J 2019 Reversible, Electric-Field Induced Magneto-Ionic Control of Magnetism in Mesoporous Cobalt Ferrite Thin Films *Sci. Rep.* **9** 1–14